Computational Materials Science 103 (2015) 170–178

Contents lists available at ScienceDirect

Computational Materials Science

journal homepage: www.elsevier.com/locate/commatsci

Cluster characteristics and physical properties of binary Al–Zr intermetallic compounds from first principles studies

Jinglian Du [a], Bin Wen [a,*], Roderick Melnik [b], Yoshiyuki Kawazoe [c,d]

[a] State Key Laboratory of Metastable Materials Science and Technology, Yanshan University, Qinhuangdao 066004, China
[b] The MS2Discovery Interdisciplinary Research Institute, Wilfrid Laurier University, 75 University Ave. West, Waterloo, Ontario N2L 3C5, Canada
[c] New Industry Creation Hatchery Center, Tohoku University, 6-6-4 Aramaki-aza-Aoba, Aoba-ku, Sendai 980-8579, Japan
[d] Institute of Thermophysics, Siberian Branch of the Russian Academy of Sciences, 1, Lavyrentyev Avenue, Novosibirsk 630090, Russia

ARTICLE INFO

Article history:
Received 8 January 2015
Received in revised form 22 March 2015
Accepted 25 March 2015
Available online 11 April 2015

Keywords:
Al–Zr intermetallics
Microstructure
Phase stability
Physical properties
First-principles study

ABSTRACT

The cluster characteristics and physical properties of binary Al–Zr intermetallics have been studied in this work by performing first principles calculations. Our investigations indicate that there is a linear dependence between the mass density and Zr-content for these Al–Zr intermetallics. Besides, the coordination number of characteristic principal clusters corresponding to these Al–Zr crystalline phases varies from 10 to 16, and the local atomic structural characteristics of Al–Zr alloys can be properly reflected via the principal clusters. Results on formation energies and elastic constants reveal that these Al–Zr intermetallics are thermodynamically and mechanically stable, among which Al_2Zr possesses the largest elastic modulus and the highest hardness. Except for $AlZr_2$ and $AlZr_3$, the other Al–Zr intermetallics are brittle phases by comparison. Furthermore, studies on electric properties suggest that all of these Al–Zr intermetallics studied here are conductive phases.

1. Introduction

Aluminum-based alloys have attracted considerable attentions during the past decades, owning to their high strength, low density, good thermal stability, superior oxidation and corrosion resistance coupled with high melting point [1–3]. Among various aluminum-based alloys, the aluminum–zirconium (Al–Zr) system has become one of a promising Al-TM systems [4–7] since the addition of Zr could optimize the properties of aluminum alloys by refining grain size and inhibiting recrystallization [8–11]. Besides, Al–Zr alloys are considered as potential candidates for structural materials used in thermal nuclear reactors due to the low absorption cross-sections for thermal neutrons [12]. Therefore, it does not come as a surprise that Al–Zr alloys have been applied extensively in many fields such as aerospace and civil engineering.

As for the ten intermetallics existed in binary Al–Zr phase diagram, their crystal structures have been reported by Potzschke et al. [13–15]. Among these Al–Zr intermetallics, $AlZr_3$, Al_3Zr_5, Al_2Zr_3, Al_4Zr_5 and Al_3Zr have been investigated successively, from which Al_3Zr is the mostly studied phase because of its supernormal role as the dispersoid precipitation and reactor core components [16,17]. In terms of the other Al–Zr intermetallics, the existing studies mainly focus on their thermodynamic properties and hydrogen adsorption properties [18–22]. For example, Saunders et al. thermodynamically characterized the binary Al–Zr alloys in 1986, with particular emphasis on the Al-rich parts [15]. Fecht et al. experimentally investigated the rules underlying the crystal-to-glass phase transition of Al–Zr system in 1989, and described the sequence of phase transformations in Al–Zr binary system [20]. Lee et al. studied the hydrogen absorption properties of Al–Zr alloys in 2000, and found that the hydrogen absorption properties of mixed Al_2Zr_3 and Al_3Zr_5 intermetallics is higher than the corresponding amorphous alloy [18]. By using a thermodynamic model, Wang et al. analyzed the phase equilibrium and thermodynamic data of Al–Zr alloy system in 2001 [14]. Riabov et al. investigated the hydrogen storage properties of Al_2Zr_3 and Al_3Zr_4 in 2002 [19]. Ghosh et al. in 2005 performed first-principles investigations on the structural energetics of binary Al–Zr intermetallics [4]. In 2008, Knipling et al. explored the performance of Al_3Zr precipitation-strengthened AlZr-based alloys [6,11]. She et al. in 2010 experimentally confirmed the intermetallics Al_3Zr_5 and Al_4Zr_5 to be high temperature phases [21]. In 2011, Ferreira et al. investigated the influence of Al_3Zr volume fraction on the corrosion behavior of Al/Al_3Zr functionally graded materials (FGM) [22]. All of these researches on the thermodynamic properties

* Corresponding author. Tel.: +86 335 8568761.
E-mail address: wenbin@ysu.edu.cn (B. Wen).

http://dx.doi.org/10.1016/j.commatsci.2015.03.039
0927-0256/

and hydrogen adsorption properties provide valuable information for the applications of Al–Zr alloys.

Although much effort has been devoted to the studies of Al–Zr intermetallics in the past decades, it is clear that analyzing the mechanical and electric properties is essential for the Al–Zr alloys that are used as structural and functional materials. In addition, understanding the local atomic structural characteristics of Al–Zr intermetallics is a prerequisite for design AlZr-based complex alloys through the "cluster-plus-glue-atom" model [23], since this cluster-based model has been successfully used to describe the complex alloy phases on the basis of the obtained principal clusters, and the atomic configurations of the stable characteristic principal clusters in the complex alloys and their crystalline derivatives remain similar to each other [24,25]. In what follows, the cluster characteristics and physical properties including thermodynamic, mechanical and electric features of binary Al–Zr intermetallics have been studied in detail by performing first principles calculations.

2. Computational methods

In this work, the first-principles calculations have been performed within the framework of electronic density functional theory (DFT), as implemented in the Vienne Ab initio Simulation Package (VASP) [26]. The generalized gradient approximation (GGA) with the Perdew–Wang (PW91) parameterization is used to describe the exchange and correlation interaction [27]. The interactions between ions and valence electrons are modeled by both the projector-augmented wave (PAW) [28] and the ultra-soft pseudo-potentials (USPP) methods [29]. The pseudopotentials employed in this work explicitly treat three valence electrons for Al ($3s^2 3p^1$) and four for Zr ($4d^2 5s^2$). The crystallographic data of these binary Al–Zr intermetallics are taken from Ref. [30], and they are listed in Table 1. A plain wave cutoff energy for 300 eV has been used. Brillouin zone integrations are modeled by a Monkhorst–Pack k-point mesh [31], and the k-point mesh of each cell has been sampled by $6 \times 6 \times 1$, $5 \times 5 \times 4$, $3 \times 2 \times 4$, $7 \times 2 \times 6$, $3 \times 3 \times 4$, $5 \times 5 \times 6$, $3 \times 3 \times 4$, $4 \times 4 \times 4$, $2 \times 2 \times 5$, $6 \times 6 \times 4$, $4 \times 4 \times 5$ and $6 \times 6 \times 6$ grids for Al_3Zr, Al_2Zr, Al_3Zr_2, AlZr, Al_4Zr_5, Al_3Zr_4, Al_2Zr_3, $P6_3/mmc$-Al_3Zr_5, $I4/mcm$-Al_3Zr_5, $P6_3/mmc$-$AlZr_2$, $I4/mcm$-$AlZr_2$ and $AlZr_3$, respectively. All structures have been fully relaxed with respect to volume as well as cell-internal and external coordinates. Besides, the first principles calculations of dynamic matrix and its Fourier transform have been performed by using density functional perturbation theory (DFPT) [32,33]. And for the DFPT calculations, the supercell of $2 \times 2 \times 2$ has been used for these Al–Zr intermetallics. The corresponding interatomic force constants (IFCs) have been obtained through VASP and PHONOPY codes [34,35].

3. Results and discussion

3.1. The structural properties

3.1.1. The structural parameters

Firstly, we optimize the crystal structures of these binary Al–Zr intermetallics. Table 1 presents the optimized lattice parameters and the corresponding mass densities, compared with previous reported values [17,30,36]. Whereafter, the variation trend of mass density with Zr-content for these binary Al–Zr intermetallics is depicted in Fig. 1, from which we can see that the correlation between Zr-contents c (at.%) and mass density ρ (kg/m^3) of these binary Al–Zr intermetallics follows a linear relation, which can be formulated as: $\rho = 3707.10c + 3083.58$. This result can be understood from the fact that the mass density of pure zirconium (6475.55 kg/m^3) is larger than that of pure aluminum (2705.62 kg/m^3).

3.1.2. The structural cluster characteristics

Considering the close connections between complex alloys and their relevant crystalline counterparts, it is essential to explore the local atomic structure features reflected by the principal cluster that obtained from the corresponding intermetallics. On the basis

Table 1
The crystallographic data and mass density for the binary Al–Zr intermetallics, calculated in this work and known from the literature.

Phase	Space group	Prototype	Pearson symbol	Unit cell lattice parameters (nm)			Mass density (kg/m^3)	Reference
Al	$Fm\bar{3}m$	Cu	cF4	a = 0.4046			2706	This work
				a = 0.4050				[30]
Al_3Zr	I4/mmm	Al_3Zr	tI16	a = 0.4015		c = 1.7369	4084	This work
				a = 0.3998		c = 1.7280	4110	[30]
Al_2Zr	$P6_3/mmc$	$MgZn_2$	hP12	a = 0.5301		c = 0.8755	4526	This work
				a = 0.5282		c = 0.8748	4420	[30]
Al_3Zr_2	Fdd2	Al_3Zr_2	oF40	a = 0.9637	b = 1.3975	c = 0.5576	4658	This work
				a = 0.9599	b = 1.3879	c = 0.5572	4790	[30]
AlZr	Cmcm	BCr	oC8	a = 0.3328	b = 1.0973	c = 0.4316	4981	This work
				a = 0.3353	b = 1.0866	c = 0.4266		[30]
Al_4Zr_5	$P6_3/mmc$	Ga_4Ti_5	hP18	a = 0.8455		c = 0.5803	5213	This work
				a = 0.8432		c = 0.5791		[30]
Al_3Zr_4	$P\bar{6}$	Al_3Zr_4	hP7	a = 0.5441		c = 0.5411	5335	This work
				a = 0.5433		c = 0.5390	5280	[30]
Al_2Zr_3	$P4_2/mnm$	Al_2Zr_3	tP20	a = 0.7671		c = 0.6970	5341	This work
				a = 0.7630		c = 0.6998	5350	[30]
Al_3Zr_5	$P6_3/mmc$	Mn_5Si_3	hP16	a = 0.8326		c = 0.5548	5355	This work
				a = 0.8184		c = 0.5702	5610	[30]
Al_3Zr_5	I4/mcm	Si_3W_5	tI32	a = 1.1067		c = 0.5395	5398	This work
				a = 1.1049		c = 0.5396		[30]
$AlZr_2$	$P6_3/mmc$	$InNi_2$	hP6	a = 0.4914		c = 0.5915	5623	This work
				a = 0.4894		c = 0.5928		[30]
$AlZr_2$	I4/mcm	Al_2Cu	tI12	a = 0.6861		c = 0.5361	5512	This work
				a = 0.6854		c = 0.5501		[30]
$AlZr_3$	$Pm\bar{3}m$	$AuCu_3$	cP4	a = 0.4384			5925	This work
				a = 0.4392				[30]
Zr	$P6_3/mmc$	Mg	hP2	a = 0.3230		c = 0.5176	6477	This work
				a = 0.3231		c = 0.5148	6487	[30]

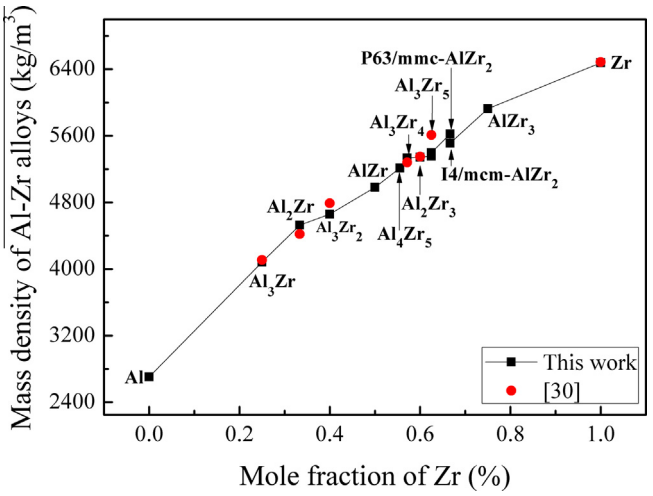

Fig. 1. The variation trend of mass density with Zr-contents for the binary Al–Zr intermetallics.

of these characteristic principal clusters, the composition design and structure description of complex alloys can be realized by virtue of the "cluster-plus-glue-atom" model, which is usually denoted via an uniform cluster formula: [cluster](glue atom)$_x$ [23,24]. Accordingly, the most representative principal clusters reflecting the cluster characteristics of Al–Zr alloys are determined from various basic primitive clusters by using our method [25]. The results indicate the characteristic principal clusters corresponding to Al_3Zr, Al_2Zr, Al_3Zr_2, AlZr, Al_4Zr_5, Al_3Zr_4, Al_2Zr_3, I4/mcm-Al_3Zr_5, P6$_3$/mmc-Al_3Zr_5, I4/mcm-$AlZr_2$, P6$_3$/mmc-$AlZr_2$ and $AlZr_3$ phases are CN12 $ZrAl_{12}$ cluster, CN16 Zr_5Al_{12} cluster, CN13 Zr_5Al_9 cluster, CN13 Zr_7Al_7 cluster, CN11 Zr_5Al_7 cluster, CN14 Zr_9Al_6 cluster CN14 Zr_9Al_6 cluster, CN10 Al_3Zr_8 cluster, CN14 Zr_9Al_6 cluster, CN10 Al_3Zr_8 cluster, CN11 Zr_7Al_5 cluster and CN12 Zr_9Al_4 cluster. Correspondingly, their respective cluster formulas are $[ZrAl_{12}]Zr_3$, $[Zr_5Al_{12}]Zr$, $[Zr_5Al_9]Zr$, $[Zr_7Al_7]$, $[Zr_5Al_7](Zr_{15/4})$, $[Zr_9Al_6]Al_{3/4}$, $[Zr_9Al_6]$, $[Al_3Zr_8]Al_{9/5}$, $[Zr_9Al_6]Zr$, $[Al_3Zr_8]Al$, $[Zr_7Al_5](Zr_3)$ and $[Zr_9Al_4]Zr_3$. Here the first atom in the cluster and cluster formula denotes the central atom of cluster. Besides, the coordination number (CN) of characteristic principal clusters in Al–Zr alloy system varies from 10 to 16. Although the characteristic principal clusters of Al_3Zr_4, Al_2Zr_3 and P6$_3$/mmc-Al_3Zr_5 phases are with the same composition, in fact their local atomic configurations are different from each other, as reflected in Fig. 2. Since the cluster information and local atomic configurations of AlZr-based complex alloys can be obtained from the closely related Al–Zr crystalline phases, it is significant to uncover the short range order features which represented by these Al–Zr characteristic principal clusters. From this viewpoint, the determination of principal clusters corresponding to these binary Al–Zr intermetallics lays the foundation for the composition design and structure description of AlZr-based complex alloy phases.

3.2. The thermodynamic properties

As is known that the equilibrium thermodynamic properties of an alloy phase can be acquired from the information of their corresponding formation and cohesive energies [37]. To achieve a better understanding of the thermodynamic properties for these Al–Zr intermetallics, we have computed and analyzed their formation energy and cohesive energy accordingly.

3.2.1. Formation energy

The difference between the total energy of Al_mZr_n and the linear combination of the pure Al and pure Zr ground state energies, is defined as the formation energy of Al_mZr_n intermetallic [5]. It can be obtained through the formula $E_{For}^{Al_mZr_n} = [E_{Tot}^{Al_mZr_n} - (mE_{Tot}^{Al} + nE_{Tot}^{Zr})]/(m+n)$. Accordingly, the formation energy of these binary Al–Zr intermetallics have been calculated and the results are presented in Fig. 3, compared with previous reported values [4,14,7,36–38]. Note that in this study we have defined the ground state convex hull by using Al_3Zr, Al_2Zr, Al_3Zr_2, Al_3Zr_4 and $AlZr_3$, since the five intermetallics are reported to be stable phases in Al–Zr alloy system at 0 K [36–38]. Besides, the calculated formation energy for AlZr, Al_2Zr_3 and $AlZr_2$ phases, which lie above the convex hull in Fig. 3, are AlZr by 1.319 kJ/mol, Al_2Zr_3 by 1.892 kJ/mol and $AlZr_2$ by 0.573 kJ/mol. Meanwhile, the AlZr and $AlZr_2$ phases have formation energy locating near to the convex hull in Fig. 3. Moreover, the calculated formation energy for Al_4Zr_5 and Al_3Zr_5 lie above the convex hull in Fig. 3 by 4.339 and 3.976 kJ/mol, respectively. These phenomena suggest that Al_4Zr_5 and Al_3Zr_5 phases are metastable at 0 K, which can be further decomposed into other more stable phases with temperature decreasing, i.e. $Al_4Zr_5 \rightarrow Al_3Zr_4 + AlZr$ and $Al_3Zr_5 \rightarrow AlZr_2 + Al_2Zr_3$ [7,21]. This is in accordance with previous studies that Al_4Zr_5 and Al_3Zr_5 are experimentally observed to be stable phases only at high temperatures. Besides, Al_2Zr possesses the largest negative formation energy among these binary Al–Zr intermetallics, which may cause an increase of its elastic modulus, this will be discussed in the following section. Furthermore, the calculated formation energy for these Al–Zr intermetallics are all negative, indicating that these binary Al–Zr intermetallics are all thermodynamically stable phases.

3.2.2. Cohesive energy

The cohesive energy which is defined to be the required energy difference between the total energy of isolated atom and the total energy of crystal unitcell, is considered as another equilibrium thermodynamic parameter to measure the stability of materials [39]. Accordingly, it should be a positive value under this definition and can be computed via $E_{Coh}^{Al_mZr_n} = [mE_{Atom}^{Al} + nE_{Atom}^{Zr} - E_{Cry}^{Al_mZr_n}]/(m+n)$, the results for the obtained cohesive energy are presented in Fig. 4, it shows clearly that the cohesive energy of these binary Al–Zr intermetallics increases with increasing Zr-content. This result implies that the structural stability of these binary Al–Zr intermetallics acsends with the increase of Zr-content, given that the stability of crystal structures can be reflected through the cohesive energy, and a larger value often implies a more stable structure [40]. Moreover, the large values of cohesive energy for these Al–Zr intermatallics also accounts for the strong chemical interactions between Al and Zr elements.

3.3. The mechanical properties

In this study, the single-crystal elastic constants are acquired to explore the mechanical properties of these Al–Zr alloy phases. Concretely, the elastic constants are computed by means of fitting the total energy density as a function of moderate strains [41]. On the basis of crystal systems and different deformation modes, the quadratic coefficient of the total energy density with respect to strain corresponds to a linear combination of certain elastic constants. And the total energy have been calculated by imposing moderate strains up to ±1.25% at 0.25% interval in our work. Table 2 gives the obtained elastic constants, from which we can see that our calculated elastic constants for $AlZr_3$ agree well with previous reported values [17]. Hitherto, there are no reported single-crystal elastic constants for the other Al–Zr intermetallics in the literatures. From this point of view, our calculated values of elastic constants for Al_3Zr, Al_2Zr, Al_3Zr_2, AlZr, Al_4Zr_5, Al_3Zr_4,

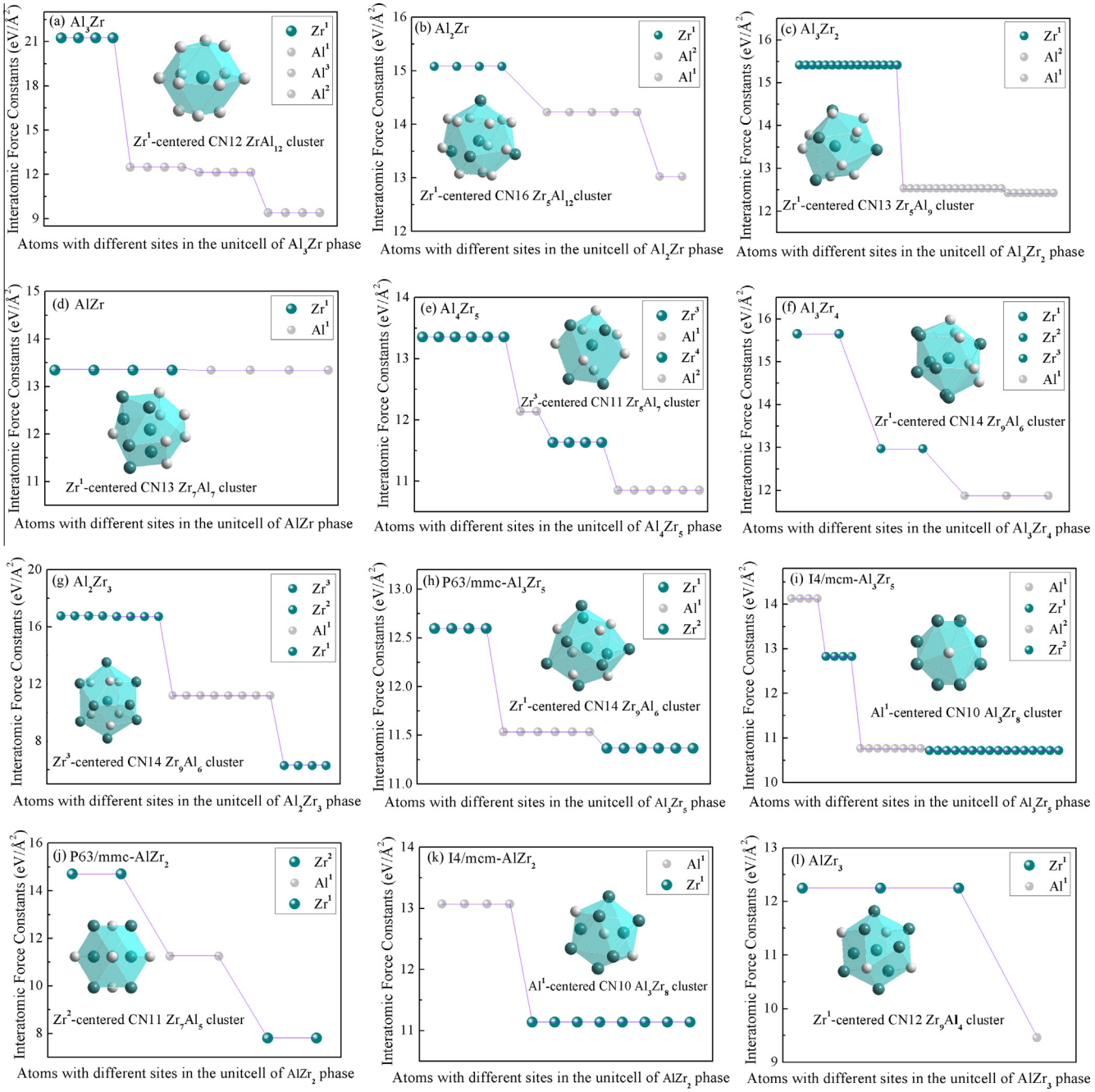

Fig. 2. The characteristic principal clusters corresponding to intermetallics in binary Al–Zr alloy system, determined from various basic primitive clusters by the interatomic force constants (eV/Å^2).

Al_2Zr_3, Al_3Zr_5 and $AlZr_2$ will provide available information for future researches on these binary Al–Zr intermetallics.

3.3.1. The mechanical stability

Next, we consider the mechanical stability of these binary Al–Zr intermetallics, on the basis of their respective single-crystal elastic constants [42]. As for the binary Al–Zr intermetallics studied in this work, $AlZr_3$ belongs to the cubic crystal system; Al_3Zr, Al_2Zr_3, I4/mcm-Al_3Zr_5 and I4/mcm-$AlZr_2$ belong to the tetragonal crystal system; Al_2Zr, Al_4Zr_5, Al_3Zr_4, P6$_3$/mmc-Al_3Zr_5 and P6$_3$/mmc-$AlZr_2$ belong to the hexagonal crystal system; while Al_3Zr_2 and AlZr belong to the orthorhombic crystal system.

For the cubic crystal system structures, the criteria of mechanical stability [42] are given as formulas (1):

$$C_{11} > 0, C_{44} > 0, C_{11} > |C_{12}|, C_{11} + 2C_{12} > 0. \quad (1)$$

The elastic constants shown in Table 2 indicate that $AlZr_3$ phase coincide with the above mechanical stability requirements, signifying it is a mechanically stable phase.

For tetragonal crystal system structures, the restrictions of mechanical stability [42] are expressed by the following formulas (2):

$$\begin{aligned} &C_{11} > 0, C_{33} > 0, C_{44} > 0, C_{66} > 0, C_{11} - C_{12} > 0, \\ &C_{11} + C_{33} - 2C_{13} > 0, 2(C_{11} + C_{12}) + C_{33} + 4C_{13} > 0. \end{aligned} \quad (2)$$

From the results listed in Table 2, we can see that all the values of elastic constants for Al_3Zr, Al_2Zr_3, I4/mcm-Al_3Zr_5 and I4/mcm-$AlZr_2$ satisfy the restrictions in formulas (2), confirming that they are mechanically stable.

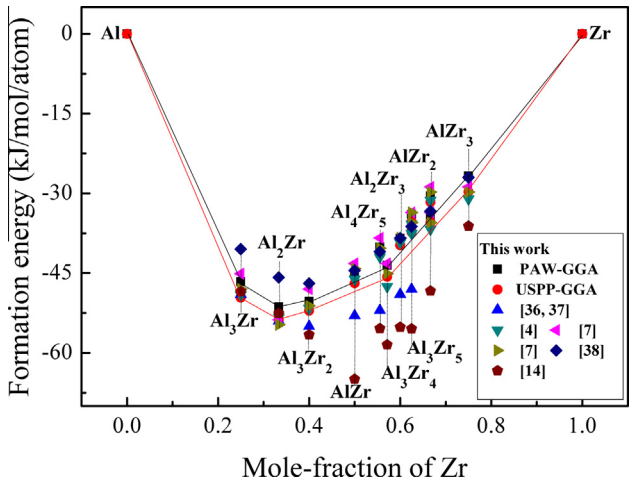

Fig. 3. The formation energy of binary Al–Zr intermetallics, compared to experimental and other theoretical values know from literature.

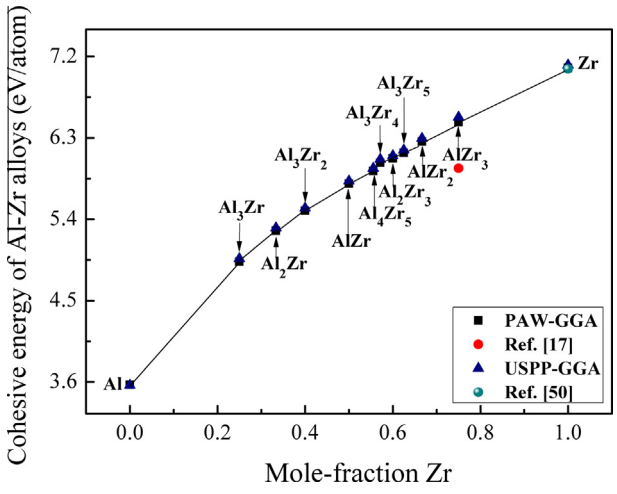

Fig. 4. The cohesive energy for the phases in binary Al–Zr alloy system.

In terms of hexagonal crystal system structures, the mechanical stability restrictions [42] are given by formulas (3):

$$C_{44} > 0, C_{11} > |C_{12}|, (C_{11} + 2C_{12})C_{33} > 2C_{13}^2. \quad (3)$$

As shown in Table 2, the elastic constants of Al_2Zr, Al_4Zr_5, $P6_3/mmc$-$AlZr_2$ and $P6_3/mmc$-Al_3Zr_5 meet the mechanical stability criteria in formulas (3), revealing that these hexagonal structures in binary Al–Zr alloy system are mechanically stable.

For orthorhombic crystal system structures, the requirements of mechanical stability [42] are represented as formulas (4):

$$C_{11} > 0, C_{22} > 0, C_{33} > 0, C_{44} > 0, C_{55} > 0,$$
$$C_{66} > 0, C_{11} + C_{22} + C_{33} + 2(C_{12} + C_{13} + C_{23}) > 0,$$
$$C_{11} + C_{22} - 2C_{12} > 0, C_{11} + C_{33} - 2C_{13} > 0, C_{22} + C_{33} - 2C_{23} > 0. \quad (4)$$

It shows in Table 2 that Al_3Zr_2 and AlZr with orthorhombic structures meet the mechanical stability requirements in formulas (4), signifying they are mechanically stable phases.

Depending on the above analysis, we conclude that all the binary Al–Zr intermetallics studied here are mechanically stable. Furthermore, despite the two intermetallics Al_3Zr_5 and Al_4Zr_5 are predicted to be high temperature stable phases [7,21], the calculated single-crystal elastic constants at 0 K also meet the mechanical stability requirements.

3.3.2. The elastic properties

The elastic moduli including bulk modulus (K), shear modulus (G) and Young's modulus (E) associated with Poisson's ratio (u) of these binary Al–Zr intermetallics have been estimated from Voigt, Reuss and Hill (VRH) approximations [43] in order to uncover the mechanical properties of the corresponding polycrystalline materials. The relevant computational formulas are as follows:

$$K_{VRH} = \frac{K_V + K_R}{2}, G_{VRH} = \frac{G_V + G_R}{2}, E_{VRH} = \frac{9 * K_{VRH}}{1 + 3K_{VRH}/G_{VRH}} \quad (5)$$

$$K_{V,R} = \frac{c_{11} + 2 * c_{12}}{3}, G_V = \frac{c_{11} - c_{12} + 3 * c_{44}}{5}, G_R = \frac{5 * (c_{11} - c_{12}) * c_{44}}{c_{44} + 3 * (c_{11} - c_{12})} \quad (6)$$

Table 3 presents the obtained results for elastic modulus of these Al–Zr alloy phases. Accordingly, the relationship between bulk modulus and Zr-contents of these Al–Zr intermetallics is depicted in Fig. 5. It shows that Al_2Zr possesses the maximum K value of 113.67 GPa among these Al–Zr intermetallics. Despite there is a certain connection between bulk modulus and mass density for most materials, the alloy phases in binary Al–Zr system do not follow this correlation [44]. Moreover, the bulk moduli deduced from VRH approximation for these Al–Zr alloys agree well with the values estimated from equation of state [4]. This accordance gives predictable results for the compressibility of these Al–Zr intermetallics. Among these Al–Zr intermetallics, Al_2Zr also has the maximum G value of 92.44 and E value of 218.18 GPa, while $AlZr_3$ possesses the minimum G value of 53.39 GPa and E value of 136.22 GPa. In reality, Young's modulus is believed as an useful parameter to predict the stiffness of phases, and a bigger

Table 2
Calculated values of single-crystal elastic constants for the binary Al–Zr intermetallics.

Phase	Single-crystal elastic constants (GPa)						Reference
Al_3Zr	C_{11} = 223.54	C_{12} = 57.27	C_{13} = 48.40	C_{33} = 194.94	C_{44} = 82.47	C_{66} = 83.44	This work
Al_2Zr	C_{11} = 240.16	C_{12} = 51.12	C_{13} = 53.96	C_{33} = 224.95	C_{44} = 92.91		This work
Al_3Zr_2	C_{11} = 226.84	C_{12} = 51.35	C_{13} = 53.93	C_{22} = 215.40	C_{23} = 59.01	C_{33} = 214.62	This work
	C_{44} = 81.52	C_{55} = 80.40	C_{66} = 78.99				
AlZr	C_{11} = 171.28	C_{12} = 50.89	C_{13} = 87.67	C_{22} = 240.81	C_{23} = 45.19	C_{33} = 204.89	This work
	C_{44} = 78.42	C_{55} = 113.76	C_{66} = 80.68				
Al_4Zr_5	C_{11} = 198.59	C_{12} = 73.06	C_{13} = 50.52	C_{33} = 196.35	C_{44} = 50.84		This work
Al_3Zr_4	C_{11} = 216.72	C_{12} = 42.93	C_{13} = 61.36	C_{33} = 199.76	C_{44} = 71.16		This work
Al_2Zr_3	C_{11} = 191.61	C_{12} = 58.43	C_{13} = 74.61	C_{33} = 164.53	C_{44} = 80.97	C_{66} = 65.01	This work
$P6_3/mmc$-Al_3Zr_5	C_{11} = 211.55	C_{12} = 61.23	C_{13} = 56.11	C_{33} = 139.97	C_{44} = 39.46		This work
$I4/mcm$-Al_3Zr_5	C_{11} = 196.81	C_{12} = 61.97	C_{13} = 63.59	C_{33} = 160.75	C_{44} = 53.51	C_{66} = 74.02	This work
$P6_3/mmc$-$AlZr_2$	C_{11} = 183.37	C_{12} = 81.27	C_{13} = 60.23	C_{33} = 180.63	C_{44} = 55.67		This work
$I4/mcm$-$AlZr_2$	C_{11} = 162.28	C_{12} = 50.50	C_{13} = 88.58	C_{33} = 135.97	C_{44} = 73.41	C_{66} = 62.11	This work
$AlZr_3$	C_{11} = 145.39	C_{12} = 79.08	C_{44} = 73.49				This work
	C_{11} = 148.65	C_{12} = 79.38	C_{44} = 70.83				[17]

Table 3
Polycrystalline shear modulus (G), bulk modulus (K), Young's modulus (E), Poisson's ratio (u), G/K ratio and hardness (H) for the binary Al–Zr intermetallics.

Phase	G (GPa)	K (GPa)	E (GPa)	u	G/K	H (GPa)	Reference
Al_3Zr	82.14	105.25	195.55	0.1903	0.7805	18.61	This work
		102.5					[4]
Al_2Zr	92.44	113.67	218.18	0.1801	0.8132	20.93	This work
		113.6					[4]
Al_3Zr_2	80.97	109.48	194.87	0.2034	0.7395	17.33	This work
		108.6					[4]
AlZr	80.28	109.12	193.41	0.2046	0.7357	17.14	This work
		108.8					[4]
Al_4Zr_5	60.11	104.49	151.31	0.2586	0.5753	10.85	This work
		103.3					[4]
Al_3Zr_4	76.60	107.16	185.59	0.2114	0.7148	16.12	This work
		107.6					[4]
Al_2Zr_3	66.71	106.96	165.69	0.2418	0.6237	12.68	This work
		107.2					[4]
$P6_3/mmc$-Al_3Zr_5	54.35	99.12	137.85	0.2682	0.5483	9.67	This work
		97.5					[4]
$I4/mcm$-Al_3Zr_5	59.94	103.22	150.67	0.2567	0.5807	10.95	This work
		103.3					[4]
$P6_3/mmc$-$AlZr_2$	55.31	105.48	141.25	0.2768	0.5243	9.27	This work
		105.2					[4]
$I4/mcm$-$AlZr_2$	51.94	101.64	133.15	0.2817	0.5110	8.67	This work
$AlZr_3$	53.39	101.18	136.22	0.2756	0.5277	9.15	This work
		101.4					[4]
	53.40	102.47	136.49	0.2780	0.5211	9.02	[17]

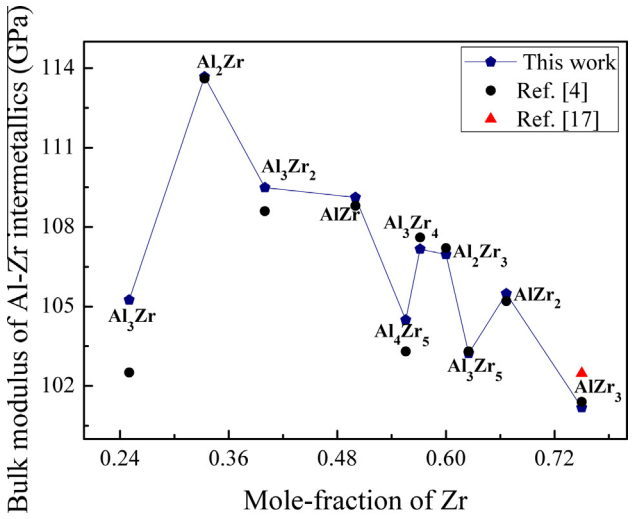

Fig. 5. The bulk modulus (K) versus Zr-contents for the binary Al–Zr intermetallics, compared with the values deduced from equation of states.

Young's modulus often signifies a stiffer phase [45]. Therefore, Al_2Zr serves as the most stiffness phase among these Al–Zr alloy phases, which is in accordance with the prediction made in above section. Furthermore, Al_2Zr has the highest hardness while $AlZr_3$ has the lowest hardness among these Al–Zr intermetallics, given that materials with larger elastic modulus often possess higher hardness [46,47].

Pugh proposed the G/K ratio as a parameter to estimate the brittle and ductile behavior of polycrystalline materials [48], and the critical value of the G/K ratio is 0.57, i.e. materials whose G/K value are larger than this threshold are brittle phases, otherwise they are ductile phases [49,50]. Thereby, the G/K values of these Al–Zr alloy phases are computed to explore their brittle and ductile behavior. The results are collected in Table 3. By comparison, we can see that the G/K values for $AlZr_3$, $AlZr_2$ and $P6_3/mmc$-Al_3Zr_5 are smaller than the threshod, signifying that they behave ductile features; while the G/K values for Al_3Zr, Al_2Zr, Al_3Zr_2, AlZr, Al_4Zr_5, Al_3Zr_4, Al_2Zr_3 and $I4/mcm$-Al_3Zr_5 are respectively 0.78, 0.81, 0.74, 0.73, 0.5753, 0.71, 0.62 and 0.58, which are bigger than 0.57, revealing that they show the brittle behavior. Being another available parameter to predict the ductility of materials, Poisson's ratio is used to measure the stability of materials against shear strain [51]. Accordingly, Fig. 6 depicts the variation of G/K ratio against Poisson's ratio for these Al–Zr intermetallics, from which we can see that these two parameters are accurately linear relation for these Al–Zr intermetallics. This linear dependence relation can be further expressed via the following formula: $G/K = -2.9761u + 1.3458$. Besides, $AlZr_2$ has the maximum u value of 0.2817, thus it should possess the best plasticity among these Al–Zr intermetallics, considering that larger u values usually signify materials with good plasticity.

3.4. The electric properties

Finally, the electronic energy band structures and density of states have been obtained to explore the electric properties of

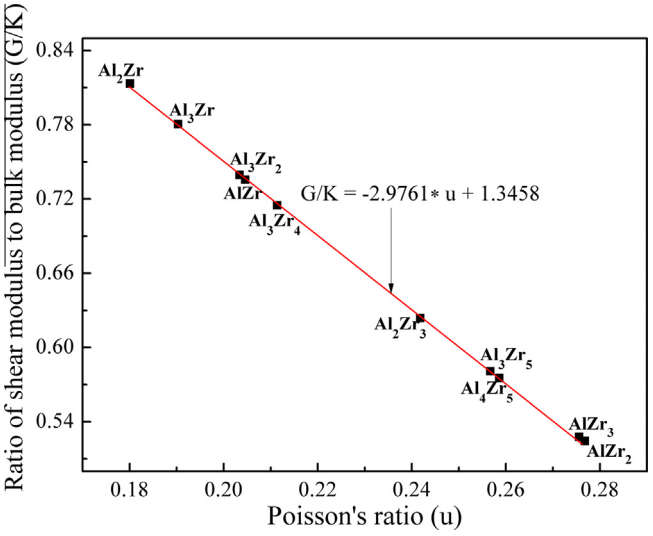

Fig. 6. The variation of Poisson's ratio (u) against the ratio of shear modulus to bulk modulus (G/K) for the binary Al–Zr intermetallics.

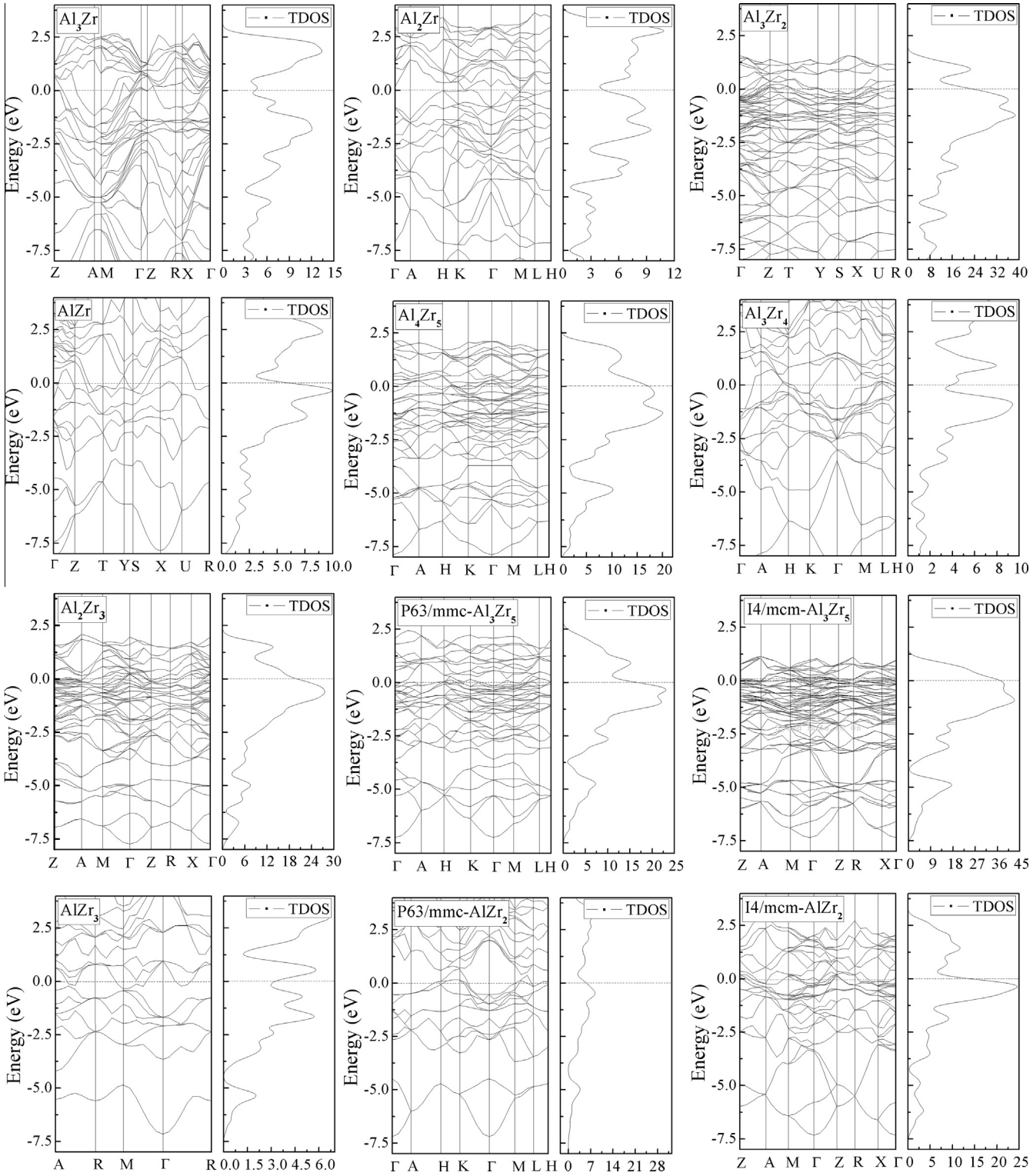

Fig. 7. The electronic energy band structures and density of states for the binary Al–Zr intermetallics.

these binary Al–Zr intermetallics. The results are depicted in Figs. 7 and 8, from which the dash-dot line of zero-point energy represents the Fermi level (E_F). As we observe in Fig. 7, the valence band overlaps the conduction band at the Fermi surface for Al_3Zr, Al_2Zr, Al_2Zr_3, Al_3Zr_2, AlZr, Al_4Zr_5, Al_3Zr_4, Al_3Zr_5, $AlZr_2$ and $AlZr_3$. This fact indicates clearly that all of these Al–Zr alloy phases studied here behave the metallic properties. In the meantime, the density of states corresponding to E_F surface is not zero, which also signifies the conductive features of these Al–Zr intermetallics. Furthermore, the bonding electron numbers per atom below E_F surface are respectively 5.249, 5.996, 6.601, 7.491, 8.007, 8.150, 8.409, 8.631, 8.993 and 9.746 for Al_3Zr, Al_2Zr, Al_3Zr_2, AlZr, Al_4Zr_5, Al_3Zr_4, Al_2Zr_3, Al_3Zr_5, $AlZr_2$ and $AlZr_3$, which reveals the variation trend of the structural stability versus Zr-contents for these Al–Zr intermetallics, given that the larger number of bonding electrons usually implies the stronger interaction between the charges and

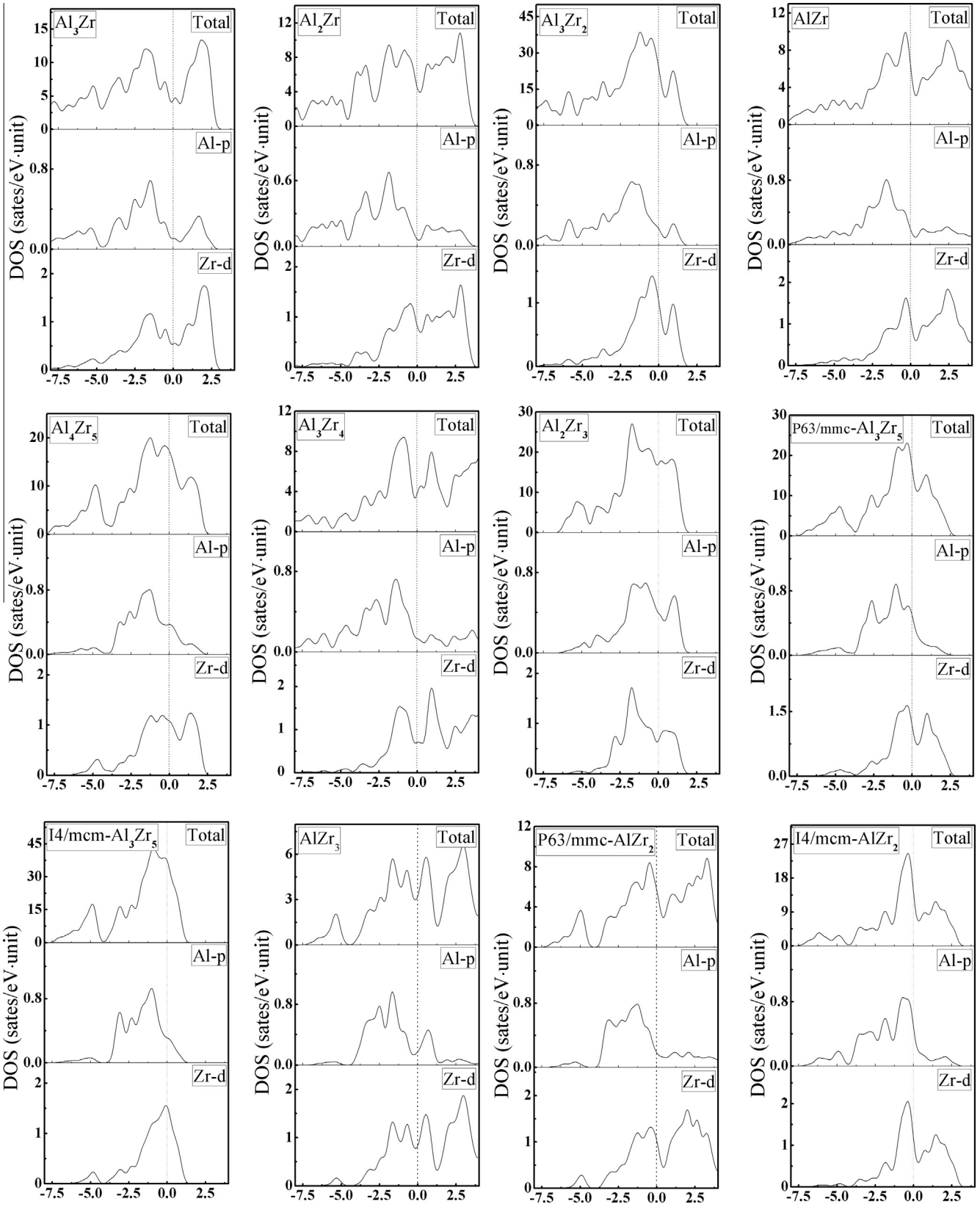

Fig. 8. The total density of states (TDOS) and partial density of states for the binary Al–Zr intermetallics.

the better structural stability of an alloy phase [52,53]. This conclusion is in accordance with the result predicted by their cohesive energy in previous sections.

As is reflected in Fig. 8, the densities of states at E_F surface for these Al–Zr intermetallics are mainly controlled by the Al-p and Zr-d electrons. Moreover, the Al-p states and Zr-d states show

evidence for hybridization in the valence band of these Al–Zr intermetallics. Below the E_F surface, the Al–Zr bonding states are occupied with the center of the valence band located at about 1.5 eV. The regions above the E_F surface constitute the conduction band, which are dominated by the Zr-d electrons for these Al–Zr alloy phases. Besides, the entire DOS curve can be divided into bonding and antibonding regions, and a pseudogap resides between them because of the strong hybridization. Researches reveals that the structural stability of a given phase can be deduced from the position of E_F level in the density of states curve [54]. Concretely, the E_F located at the valley in the bonding states implies that the phase is with good stability, while the E_F that lies on the valley in the antibonding region suggests the phase is metastable [55]. As is shown in Fig. 8, the E_F lies to the left of the pseudogap for most of the Al–Zr intermetallics studied here, indicating they are the structurally stable phases. While for Al_4Zr_5 and Al_3Zr_5, their E_F lies to the right of the pseudogap in the DOS curve, suggesting they are the metastable phases and will decompose into other stable phases. This is in line with the conclusion made from the thermodynamic analysis and the experimental investigations [7,21].

4. Conclusion

In summary, we have performed first-principles calculations to investigate the cluster characteristics and physical properties including thermodynamic, mechanical together with electric features of binary Al–Zr intermetallics. The results indicated that the coordination number of the characteristic principal clusters corresponding to these binary Al–Zr crystallines varies from 10 to 16. Besides, there is a linear dependence between mass density and Zr-content of these Al–Zr alloys. Results on formation energies and elastic constants suggest that these Al–Zr intermetallics are thermodynamically and mechanically stable phases. Furthermore, the polycrystalline elastic moduli of these Al–Zr intermetallics have been deduced from their respective single-crystal elastic constants via VRH approximations. Among these binary Al–Zr intermetallics, Al_2Zr phase possesses the largest elastic modulus and the highest hardness. Meanwhile, there is a linear correlation between the Poisson's ratio and G/K ratios for these Al–Zr intermetallics. With the increasing Zr-content, the cohesive energy of these Al–Zr alloy phases enhances. Analysis on energy band structures and density of states suggest that all of these Al–Zr intermetallics studied here behave the metallic conductive properties.

Acknowledgments

This work was supported by the National Natural Science Foundation of China (Grant Nos. 51121061, 51131002), the Key Basic Research Program of Hebei Province of China (Grant No. 12965135D) and the Natural Science Foundation for Distinguished Young Scholars of Hebei Province of China (Grant No. E2013203265). R.M. acknowledges the support from the NSERC and CRC programs, Canada. The authors also would like to thank the staff of the Center for Computational Materials Science, Institute for Materials Research, Tohoku University for computer support. Y.K. is thankful to the CREST project headed by Prof. M. Kotani.

References

[1] W. Miao, K. Tao, B. Li, B.X. Liu, J. Phys. D – Appl. Phys. 33 (2000) 2300.
[2] K.I. Moon, K.Y. Chang, K.S. Lee, J. Alloys Compd. 312 (2000) 273.
[3] B. Wen, J.J. Zhao, F.D. Bai, T.J. Li, Intermetallics 16 (2008) 333.
[4] G. Ghosh, M. Asta, Acta Mater. 53 (2005) 3225.
[5] C. Wolverton, V. Ozoliņš, Phys. Rev. B 73 (2006) 144104.
[6] K.E. Knipling, D.C. Dunand, D.N. Seidman, Acta Mater. 56 (2008) 114.
[7] M. Alatalo, M. Weinert, R.E. Watson, Phys. Rev. B 57 (1998) R2009.
[8] C.B. Fuller, D.N. Seidman, D.C. Dunand, Acta Mater. 51 (2003) 4803.
[9] A. Laik, K. Bhanumurthy, G.B. Kale, Intermetallics 12 (2004) 69.
[10] V. Rigaud, B. Sundman, D. Daloz, G. Lesoult, Calphad 33 (2009) 442.
[11] K.E. Knipling, D.C. Dunand, D.N. Seidman, Acta Mater. 56 (2008) 1182.
[12] B. Srinivasarao, C. Suryanarayana, K. Oh-ishi, K. Hono, Mater. Sci. Eng. A 518 (2009) 100.
[13] M. Potzschke, K. Schubert, Z Metallkd 53 (1962) 548.
[14] T. Wang, Z.P. Jin, J.C. Zhao, J. Phase Equilib. 22 (2001) 544.
[15] N. Saunders, V.G. Rivlin, Mater. Sci. Technol. 2 (1986) 521.
[16] G. Ghosh, S. Vaynman, M. Asta, M.E. Fine, Intermetallics 15 (2007) 44.
[17] Y.Z. Guan, H.Y. Zhang, W. Li, Phys. B – Condens. Matter 406 (2011) 1149.
[18] S.M. Lee, Y.J. Park, H.Y. Lee, K.C. Kim, H.K. Baik, Intermetallics 8 (2000) 781.
[19] A.B. Riabov, V.A. Yartys, R.V. Denys, B.C. Hauback, J. Alloys Compd. 356–357 (2003) 91.
[20] H.J. Fecht, G. Han, Z. Fu, W.L. Johnson, J. Appl. Phys. 67 (1990) 1744.
[21] J. She, Y. Zhan, Z. Hu, C. Li, J. Hu, Y. Du, H. Xu, J. Alloys Compd. 497 (2010) 118.
[22] S.C. Ferreira, L.A. Rocha, E. Ariza, P.D. Sequeira, Y. Watanabe, J.C.S. Fernandes, Corros. Sci. 53 (2011) 2058.
[23] C. Dong, Q. Wang, J.B. Qiang, Y.M. Wang, N. Jiang, G. Han, et al., J. Phys. D – Appl. Phys. 40 (2007) 273.
[24] G. Han, J.B. Qiang, F.W. Li, L. Yuan, S.G. Quan, Q. Wang, Acta Mater. 59 (2011) 5917.
[25] J.L. Du, B. Wen, R. Melnik, Y. Kawazoe, Acta Mater. 75 (2014) 113.
[26] G. Kresse, M. Marsman, J. Furthüller, VASP the guide, <http://cms.mpi.Univie.ac.at/vasp/>.
[27] M.C. Payne, M.P. Teter, D.C. Allan, T.A. Arias, J.D. Joannopoulous, Rev. Mod. Phys. 64 (1992) 1045.
[28] P.E. Blöchl, Phys. Rev. B 50 (1994) 17953.
[29] D. Vanderbilt, Phys. Rev. B 41 (1990) 7892.
[30] P. Villars, L.D. Calvert, Pearson's Handbook of Crystallographic Data for Intermetallic Phases, ASM International, Materials Park (OH), 1997.
[31] H.J. Monkhorst, J.D. Pack, Phys. Rev. B 13 (1976) 5188.
[32] S. Baroni, P. Giannozzi, A. Testa, Phys. Rev. Lett. 58 (1987) 1861.
[33] X. Gonze, D.C. Allan, M.P. Teter, Phys. Rev. Lett. 68 (1992) 3603.
[34] A. Togo, F. Oba, I. Tanaka, Phys. Rev. B 78 (2008) 134106.
[35] A. Togo, Phonopy, <http://phonopy.sourcefore.net/>.
[36] R.J. Kematic, H.F. Franzen, J. Solid State Chem. 54 (1984) 226.
[37] J. Murray, A. Peruzzi, J.P. Abriata, J. Phase Equilib. 13 (1992) 277.
[38] N. Saunders, Z Metallkd 80 (1989) 894.
[39] V.I. Razumovskiy, A.V. Ruban, I.M. Razumovskii, A.Y. Lozovoi, V.N. Butrim, Yu.Kh. Vekilov, Scr. Mater. 65 (2011) 926.
[40] C. Kittel, P. McEuen, Introduction to Solid State Physics, Wiley, New York, 1996.
[41] B. Wen, T. Shao, R. Melnik, Y. Kawazoe, Y. Tian, J. Appl. Phys. 113 (2013) 103501.
[42] Z.J. Wu, E.J. Zhao, H.P. Xiang, X.F. Hao, X.J. Liu, J. Meng, Phys. Rev. B 76 (2007) 054115.
[43] O.L. Anderson, J. Phys. Chem. Solids 24 (1963) 909.
[44] S. Pauly, Acta Mater. 57 (2009) 5445.
[45] R. Sahara, T. Shishido, A. Nomura, K. Kudou, S. Okada, V. Kumar, K. Nakajima, Y. Kawazoe, Phys. Rev. B 76 (2007) 0241051.
[46] J. Haines, J.M. Leger, G. Bocquillon, Ann. Rev. Mater. Res. 31 (2001) 1.
[47] X.Q. Chen, H.Y. Niu, D.Z. Li, Y.Y. Li, Intermetallics 19 (2011) 1275.
[48] S.F. Pugh, Philos. Mag. 45 (1954) 823.
[49] D.G. Sangiovanni, V. Chirita, L. Hultman, Phys. Rev. B 81 (2010) 104107.
[50] J.L. Du, B. Wen, R. Melnik, Y. Kawazoe, Intermetallics 54 (2014) 110.
[51] G.N. Greaves, A.L. Greer, R.S. Lakes, T. Rouxel, Nat. Mater. 10 (2011) 823.
[52] R. Hoffmann, Rev. Mod. Phys. 60 (1988) 601.
[53] Y. Zhou, B. Wen, Y.Q. Ma, R. Melnik, X.J. Liu, J. Solid State Chem. 187 (2012) 211.
[54] P. Ravindran, R. Asokamani, Bull. Mater. Sci. 20 (1997) 613.
[55] T. Hong, T.J.W. Yang, X.Q. Guo, A.J. Freeman, T. Oguchi, J.H. Xu, Phys. Rev. B 43 (1991) 1940.